



Research article

Influence of magnetic field-dependent viscosity on Casson-based nanofluid boundary layers: A comprehensive analysis using Lie group and spectral quasi-linearization method

N. Vishnu Ganesh^a, B. Rajesh^a, Qasem M. Al-Mdallal^{b,*}, Hillary Muzara^c^a PG and Research Department of Mathematics, Ramakrishna Mission Vivekananda College, Mylapore, Chennai -600004, Tamil Nadu, India^b Department of Mathematical Sciences, United Arab Emirates University, P.O. Box 15551, Al Ain, Abu Dhabi, United Arab Emirates^c Department of Mathematics and Computational Sciences, University of Zimbabwe, Zimbabwe

ARTICLE INFO

Keywords:

Boundary layer flow
Casson nanofluid
Lie group
MFD viscosity
SQLM

ABSTRACT

This study examines the effects of magnetic-field-dependent (MFD) viscosity on the boundary layer flow of a non-Newtonian sodium alginate-based Fe_3O_4 nanofluid over an impermeable stretching surface. The non-Newtonian Casson and homogeneous nanofluid models are utilized to derive the governing flow and heat transfer equations. Applying Lie group transformations to dimensional partial differential equations yields nondimensional ordinary differential equations, which are then numerically solved using the spectral quasi-linearization technique. The analysis primarily focuses on the impacts of the MFD viscosity parameter, nanoparticle volume fraction of Fe_3O_4 , and magnetic parameters on the flow and heat transfer characteristics. The local skin friction and heat transfer rate behaviors influenced by viscosity changes due to the magnetic field are discussed. It is found that MFD viscosity significantly impacts flow and thermal energies, enhancing skin friction coefficients and reducing Nusselt numbers in the boundary layer region.

1. Introduction

In the fields of aerodynamics, chemical engineering, manufacturing, and other engineering disciplines, it is crucial to investigate the heat transfer properties of boundary layer flows involving both Newtonian and non-Newtonian fluids. Boundary layer flows occur when a fluid moves in close proximity to a solid surface, creating velocity gradients and shear stresses within this thin layer. These flows have been extensively studied assuming Newtonian fluid behavior, where viscosity remains constant regardless of the shear rate [1–4]. However, real-world fluids often deviate from this ideal behavior, displaying characteristics such as shear thinning, thickening, viscoelasticity, and yield stress, making the understanding and prediction of flow and heat transfer behaviors challenging. This is especially relevant since numerous engineering applications require the study of non-Newtonian fluids in boundary layer flow with heat transfer, as they significantly influence flow characteristics and heat transfer performance. One intriguing scenario in this context is the flow of non-Newtonian fluids over a stretching sheet. This topic finds applications in various fields such as polymer processing, thin film coating and deposition, biomedical engineering, microfluidics, heat and energy transfer systems, surface coatings and functionalization, aerospace, and aeronautics [5–10].

* Corresponding author.

E-mail addresses: nvishnuganeshmath@gmail.com (N. Vishnu Ganesh), q.almhdallal@uaeu.ac.ae (Q.M. Al-Mdallal).

<https://doi.org/10.1016/j.heliyon.2024.e28994>

Received 9 October 2023; Received in revised form 24 March 2024; Accepted 27 March 2024

Available online 3 April 2024

2405-8440/© 2024 The Author(s). Published by Elsevier Ltd. This is an open access article under the CC BY-NC-ND license (<http://creativecommons.org/licenses/by-nc-nd/4.0/>).

Nomenclature

(u^*, v^*)	Velocity components.....	ms^{-1}	k	Fluid thermal conductivity.....	$\text{W m}^{-1} \text{K}^{-1}$
(x^*, y^*)	Coordinates of the surface.....	m	ρC_p	Specific heat capacitance	$\text{J m}^{-3} \text{K}^{-1}$
u_w^*	Stretching velocity	ms^{-1}	Pr	Prandtl number	
e_{mn}	Deformation rate component		C_f	Coefficient of skin friction	
π_{ct}	Critical value of the fluid		Nu_{x^*}	Nusselt number	
r_y	Yield stress		τ_w	Shear stress at the wall	
μ_D	Dynamic viscosity	kg (ms)^{-1}	Re_{x^*}	Local Reynolds number	
$\bar{\delta}$	MFD Viscosity variation		T_w^*	Temperature at the stretching field.....	K
B_0	Magnetic field strength		T_∞^*	Temperature far from the stretching field	K
β	Casson parameter		<i>Subscript</i>		
ν	Kinetic viscosity	m^2s^{-1}	s	Nanoparticles	
σ	Electric conductivity	S m^{-1}	f	Base fluid	
ρ	Fluid density.....	kg m^{-3}	nf	Nanofluid	
ϕ	Volume fraction of nanoparticles				

Casson fluids, known for their ability to capture shear-thinning behavior, exhibit unique characteristics when subjected to stretching. These fluids flow below their yield stress, and their viscosity decreases with increasing shear rate. The stretching sheet velocity profiles, shear stresses, and heat transfer characteristics of a stretching sheet in contact with Casson fluids depend on their rheological features. Nanofluids, which are suspensions of nanoparticles in base fluids, seamlessly integrate nanotechnology into their composition. They are highly desirable for heat transfer applications because of their exceptional thermal conductivity and efficiency [11]. Investigating Casson nanofluids over a stretching sheet provides valuable insights into their flow and heat transmission properties, generating significant interest in the field of fluid dynamics and heat transfer [12–22].

Magnetohydrodynamics (MHD), which combines fluid dynamics and electromagnetism, is used to understand the behavior of electrically conducting fluids in magnetic fields. This interdisciplinary field uncovers a wide range of phenomena that involve the interplay between magnetic fields and fluid flows, extending beyond traditional fluid dynamics. The study of electrically conducting non-Newtonian fluids under the influence of a magnetic field holds significance in numerous engineering and technological domains. These applications span disciplines, including turbomachinery, nuclear reactor cooling, heat exchanger design, nuclear acceleration device assembly, and blood-flow measurement techniques [23–29]. For instance, Sulochana et al. [30] conducted a comparative analysis of the three-dimensional (3D) flow of Newtonian and non-Newtonian MHD Casson nanofluids over a stretching sheet under convective boundary conditions. Their study revealed that the non-Newtonian Casson nanofluid exhibited superior rates of heat and mass transfer compared to Newtonian nanofluids. Similarly, Sabir et al. [31] investigated the flow behavior of a two-phase nanofluid over a stretching sheet in the presence of a magnetic field, chemical reactions, and gyrotactic micro-organisms, with a particular focus on the boundary layer. Their findings highlighted the increasing impact of magnetic parameters on the local Nusselt number. Nadeem et al. [32] scrutinized the MHD 3D boundary layer flow of a Casson nanofluid across a linearly stretched surface. Furthermore, Mustafa et al. [33] analyzed the flow characteristics of a two-phase Casson nanofluid over a nonlinearly stretched sheet, considering the effects of varying magnetic fields and observed an increasing trend in temperature with the Casson parameter. Khan et al. [34] investigated the time-dependent homogeneous flow of sodium alginate-Casson nanofluids on a vertically-heated plate, emphasizing the influence of magnetic fields and thermal radiation. Ghadikolaei et al. [35] explored mixed convection flow of an MHD two-phase Casson nanofluid, considering the effects of nonlinear thermal radiation. Ramudu et al. [36] studied the effect of Brownian motion on heat and mass transfer in an MHD two-phase Casson nanofluid flow over a stretched sheet with nonlinear thermal radiation. Alwawi et al. [37] examined the MHD free-convection flow of sodium alginate-based nanofluids containing various nanoparticles around a sphere and found that the silver nanofluid exhibited higher temperatures than others. Panigrahi et al. [38] conducted a comprehensive review of the heat and mass transfer properties of MHD two-phase Casson nanofluids in a porous medium with chemical reactions, convective boundary conditions, and non-uniform heat sink/source, considering the influence of thermal radiation. Their analysis revealed a decreasing temperature profile with an increase in the Casson parameters. Jamshed et al. [39] investigated the flow characteristics of a single-phase Casson nanofluid based on ethylene glycol with copper and molybdenum disulfide nanoparticles over a stretching sheet, considering an inclined magnetic field, viscous and ohmic dissipations, and entropy generation. Kumar et al. [40] examined the two-phase MHD flow of a Casson nanofluid over a surface with exponential stretching velocity, incorporating activation energy, thermal radiation, and Hall current effects. Reddy and Maddileti [41] studied the MHD two-phase flow of a Casson nanofluid with temperature-dependent viscosity and thermal conductivity over a stretching sheet, reporting enhanced temperature and concentration profiles using the Casson parameter. Sekar et al. [42] focused on the impact of the Soret and Dufour effects on the boundary layer flow of an MHD two-phase Casson nanofluid over a nonlinearly stretched, inclined surface. Rani et al. [43] explored the effects of various nanoparticle shapes, including spherical, brick, blade, and platelet-shaped copper nanoparticles, in a sodium alginate-based Casson nanofluid, considering the implications of the magnetic field. They concluded that an increase in the Casson parameter led to elevated temperatures for all the nanoparticle shapes in the presence of a magnetic field.

Magnetic-field-dependent (MFD) viscosity shows how magnetic fields influence fluid flow. In classical fluid dynamics, viscosity is typically assumed to be constant and unaffected by external variables. The strength and orientation of the magnetic field can affect

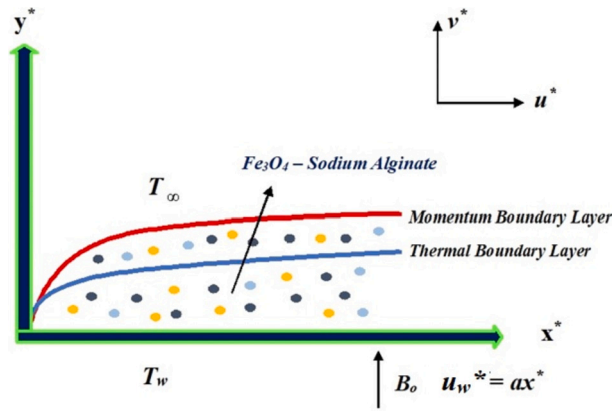


Fig. 1. Physical configuration of the present model.

the viscosity of the conducting fluid. MFD arises from the interaction of the magnetic field with charged particles in the fluid, altering internal friction and flow behavior. Understanding and quantifying MFD viscosity is of great importance with broad scientific and engineering implications. In fields such as astrophysics and plasma physics, accurate models that account for MHD and viscosity fluctuations are necessary to explain magnetized plasmas. In engineering and industry, magnetic fields can be harnessed to control and manipulate conducting fluid flows, thereby enhancing efficiency and performance. To illustrate this, Sheikholeslami et al. [44] explored the effects of MFD viscosity on a two-dimensional (2D), incompressible water-based alumina nanofluid flow within a square container. Their findings indicated a decrease in temperature within the enclosure with increasing magnetic viscosity. Similarly, Sheikholeslami and Sadoughi et al. [45] examined the effects of the MFD viscosity and shape factor of Fe_3O_4 nanoparticles on the behavior of water-based Fe_3O_4 nanofluids within a porous square enclosure. Their investigation revealed that platelet-shaped nanoparticles exhibit the highest Nusselt number in the presence of high MFD viscosity. Molana et al. [46] delved into the effects of the MFD viscosity on the natural convective flow of a water-based Fe_3O_4 nanofluid in a novel porous cavity.

However, after an extensive review of the existing literature, it becomes evident that no prior studies have explored the impact of viscosity dependence on the magnetic field in the context of natural convection flow of a sodium alginate Casson-based magnetite nanofluid over a stretching sheet. This is surprising given the considerable potential of this area of research to enhance heat transfer, improve energy efficiency, optimize industrial processes, facilitate material processing, and advance renewable energy. In light of this gap, the current study conducted fundamental experiments to investigate the influence of MFD viscosity on the natural convection flow of a steady non-Newtonian fluid composed of sodium alginate and Fe_3O_4 nanoparticles over a stretched surface. To address this problem, the governing equations were non-dimensionalized using Lie group transformations. The resulting set of nonlinear coupled non-dimensional equations was solved using a highly efficient spectral quasi-linearization technique (SQLM).

2. Problem description

The problem involves examining the laminar, steady, 2D, incompressible flow of a Casson-based Fe_3O_4 nanofluid over an impermeable stretching surface that experiences a stretching velocity $u_w^* = ax^*$ (see Fig. 1). The Casson fluid model is described by the following rheological equation [15]:

$$\tau_{mn} = \begin{cases} 2(\mu_D + r_y(2\pi_{ct})^{-0.5})e_{mn}, & \pi < \pi_{ct}, \\ 2(\mu_D + r_y(2\pi)^{-0.5})e_{mn}, & \pi > \pi_{ct}, \end{cases} \quad (1)$$

where μ_D , e_{mn} , and π_{ct} indicate the dynamic viscosity, deformation rate component, critical value (dependent on the fluid model), and yield stress (r_y), respectively. Additionally, $\pi = e_{mn}e_{mn}$. The working fluid under consideration consists of electrically-conducting sodium alginate and Fe_3O_4 nanoparticle suspension. The dynamic plastic viscosity of a Casson fluid was described as $\mu = (r_y(2\pi)^{-0.5} + \mu_D)$, ($\pi_{ct} < \pi$). By employing a rheological model (see Equation (1)), the kinematic viscosity of the Casson fluid is expressed as $\nu = \frac{\mu_D}{\rho} \left(1 + \frac{1}{\beta}\right)$, where $\beta = \left(\frac{\mu_D(2\pi)^{0.5}}{r_y}\right)$ denotes Casson parameter. The kinematic viscosity of the sodium alginate Casson-based Fe_3O_4 nanofluid is derived as $\nu_{nf} = \frac{\mu_{nf}}{\rho_{nf}} \left(1 + \frac{1}{\beta}\right)$. The nanofluids viscosity is expected to vary due to the magnetic field and is described as follows: [44,45]

$$\eta_{nf} = (1 + \bar{\delta} \cdot \bar{B})\mu_{nf}, \quad (2)$$

where $\bar{\delta}$ represents the viscosity variation caused by the applied magnetic field, and it is assumed to be isotropic. Furthermore, ($\bar{\delta} = \delta$), and \bar{B} denotes the magnetic field intensity. Using Equation (2), the MFD kinematic viscosity of the Casson-based nanofluid is expressed as follows:

Table 1
Thermo-physical properties of fluid and nanoparticles.

	ρ (kg/m ³)	C_p (J/kg K)	k (W/m K)	σ (Ω m) ⁻¹
Fe ₃ O ₄	5180	670	9.7	25000
Sodium alginate	989	4175	0.6376	0.05

$$v_{nf} = \frac{\eta_{nf}}{\rho_{nf}} \left(1 + \frac{1}{\beta}\right) = \frac{(1 + \bar{\delta} \cdot \bar{B})\mu_{nf}}{\rho_{nf}} \left(1 + \frac{1}{\beta}\right). \tag{3}$$

The axes labeled x^* and y^* remain fixed relative to the stretching surface and are oriented perpendicular to it. Temperature at the stretching and far fields is denoted by T_w^* and T_∞^* , respectively. A uniform magnetic field of intensity B_0 is applied transversely, with negligible electric field intensity and magnetic Reynolds number. Furthermore, it is assumed that there was no slip between the base fluid and Fe_3O_4 nanoparticles, and both are in a state of thermal equilibrium. Table 1 lists the thermophysical characteristics of the working fluid and nanoparticles.

By considering the aforementioned assumptions and applying the conventional boundary layer approximation alongside Equation (3), the governing equations that describe the mass, momentum, and energy of a non-Newtonian (Casson)-based homogeneous Fe_3O_4 nanofluid are derived, considering the influential effects of the MFD viscosity as follows [17]:

$$\frac{\partial u^*}{\partial x^*} + \frac{\partial v^*}{\partial y^*} = 0, \tag{4}$$

$$u^* \frac{\partial u^*}{\partial x^*} + v^* \frac{\partial u^*}{\partial y^*} - \left(1 + \frac{1}{\beta}\right) \frac{\eta_{nf}}{\rho_{nf}} \frac{\partial^2 u^*}{\partial y^{*2}} + \frac{\sigma_{nf} B_0^2 u^*}{\rho_{nf}} = 0, \tag{5}$$

$$u^* \frac{\partial T^*}{\partial x^*} + v^* \frac{\partial T^*}{\partial y^*} - \frac{k_{nf}}{(\rho C_p)_{nf}} \frac{\partial^2 T^*}{\partial y^{*2}} = 0, \tag{6}$$

where the velocities u^* and v^* are along the x^* and y^* directions, respectively, and T^* represents the local temperature of the fluid. The corresponding dimensional boundary conditions for Equations (4)–(6) are as follows:

$$u^* = u_w^*(x^*) = ax^*, \quad v^* = 0, \quad T^* = T_w^*, \quad \text{at } y^* = 0, \tag{7}$$

$$u^* \rightarrow 0, \quad T^* \rightarrow T_\infty^*, \quad \text{as } y^* \rightarrow \infty.$$

3. Thermo-physical properties of nanofluid

The effective density (ρ_{nf}), effective dynamic viscosity (μ_{nf}), specific heat capacitance $(\rho C_p)_{nf}$, effective thermal conductivity (k_{nf}) and effective electric conductivity $\left(\frac{\sigma_{nf}}{\sigma_f}\right)$ of the nanofluid are all expressed as functions of the nanoparticle volume fraction ϕ , as documented in [44]:

$$\frac{\rho_{nf}}{\rho_f} = (1 - \phi) + \phi \frac{\rho_s}{\rho_f}, \quad \frac{\mu_{nf}}{\mu_f} = (1 - \phi)^{-2.5}, \tag{8}$$

$$\frac{(\rho C_p)_{nf}}{(\rho C_p)_f} = (1 - \phi) + \phi \frac{(\rho C_p)_s}{(\rho C_p)_f}, \tag{9}$$

$$\frac{k_{nf}}{k_f} = \left[\frac{k_s + 2k_f - 2\phi(k_f - k_s)}{k_s + 2k_f + \phi(k_f - k_s)} \right], \tag{10}$$

and

$$\frac{\sigma_{nf}}{\sigma_f} = 1 + \frac{3\left(\frac{\sigma_s}{\sigma_f} - 1\right)\phi}{\left(\frac{\sigma_s}{\sigma_f}\right) + 2 - \left(\frac{\sigma_s}{\sigma_f} - 1\right)\phi}. \tag{11}$$

4. Non-dimensionalization and Lie group transformations

Now, incorporating the aforementioned nondimensional variables,

$$x = (v_f/a)^{-\frac{1}{2}} x^*; \quad y = (v_f/a)^{-\frac{1}{2}} y^*; \quad u = (v_f/a)^{-\frac{1}{2}} u^*; \tag{12}$$

$$v = (v_f/a)^{-\frac{1}{2}} v^*; \quad \theta = (T^* - T_\infty^*)(T_w^* - T_\infty^*)^{-1}.$$

Using Equations (8) - (12), the Equations (4), (5) and (6) transforms to

$$\frac{\partial u}{\partial x} + \frac{\partial v}{\partial y} = 0, \tag{13}$$

$$u \frac{\partial u}{\partial x} + v \frac{\partial u}{\partial y} - \frac{(1 + \frac{1}{\beta})(1 + \delta^*)}{(1 - \phi)^{2.5}((1 - \phi) + \phi \frac{\rho_s}{\rho_f})} \frac{\partial^2 u}{\partial y^2} + \frac{\sigma_{nf}}{\sigma_f} \frac{Mu}{((1 - \phi) + \phi \frac{\rho_s}{\rho_f})} = 0, \tag{14}$$

$$u \frac{\partial \theta}{\partial x} + v \frac{\partial \theta}{\partial y} - \frac{k_{nf}}{k_f Pr} \frac{1}{((1 - \phi) + \phi \frac{(\rho C_p)_s}{(\rho C_p)_f})} \frac{\partial^2 \theta}{\partial y^2} = 0, \tag{15}$$

and the boundary conditions in Equation (7) transformed to

$$u = x, \quad v = 0, \quad \theta = 1, \quad \text{at } y = 0, \tag{16}$$

$$u \rightarrow 0, \quad \theta \rightarrow 0, \quad \text{as } y \rightarrow \infty,$$

where $\delta^* = \delta B_0$ represents the viscosity parameter, $M = \sigma_f B_0^2 (\rho_f a)^{-1}$ is the magnetic parameter, and $Pr = \frac{\nu_f}{\alpha_f}$ denotes the Prandtl number of the base fluid. The stream function, ψ , which satisfies Equation (13) and is specified as $u = \frac{\partial \psi}{\partial y}$ and $v = -\frac{\partial \psi}{\partial x}$. The Equations (14)- (16) can be expressed in terms of stream function as follows:

$$\frac{\partial \psi}{\partial y} \frac{\partial^2 \psi}{\partial x \partial y} - \frac{\partial \psi}{\partial x} \frac{\partial^2 \psi}{\partial y^2} - \frac{(1 + \frac{1}{\beta})(1 + \delta^*)}{(1 - \phi)^{2.5}((1 - \phi) + \phi \frac{\rho_s}{\rho_f})} \frac{\partial^3 \psi}{\partial y^3} + \frac{\sigma_{nf}}{\sigma_f} \frac{Mu}{((1 - \phi) + \phi \frac{\rho_s}{\rho_f})} \frac{\partial \psi}{\partial y} = 0, \tag{17}$$

$$\frac{\partial \psi}{\partial y} \frac{\partial \theta}{\partial x} - \frac{\partial \psi}{\partial x} \frac{\partial \theta}{\partial y} - \frac{k_{nf}}{k_f Pr} \frac{1}{((1 - \phi) + \phi \frac{(\rho C_p)_s}{(\rho C_p)_f})} \frac{\partial^2 \theta}{\partial y^2} = 0, \tag{18}$$

with the boundary conditions

$$\frac{\partial \psi}{\partial y} = x, \quad \frac{\partial \psi}{\partial x} = 0, \quad \theta = 1, \quad \text{at } y = 0, \tag{19}$$

$$\frac{\partial \psi}{\partial y} \rightarrow 0, \quad \theta \rightarrow 0, \quad \text{as } y \rightarrow \infty.$$

By utilizing the following Lie-group transformations [47]

$$y = \eta, \psi = x f(\eta), \theta = \theta(\eta),$$

in Equations (17) - (19), the following non-dimensional ODE's and the boundary conditions are obtained:

$$(1 + \frac{1}{\beta})(1 + \delta^*) f''' + (1 - \phi)^{2.5}((1 - \phi) + \phi \frac{\rho_s}{\rho_f}) [f f'' - f'^2] = (1 - \phi)^{2.5} \frac{\sigma_{nf}}{\sigma_f} M f', \tag{20}$$

$$\frac{k_{nf}}{k_f Pr} \frac{1}{((1 - \phi) + \phi \frac{(\rho C_p)_s}{(\rho C_p)_f})} \theta'' + f \theta' = 0, \tag{21}$$

$$f(\eta) = 0, \quad f'(\eta) = 1, \quad \theta(0) = 1, \quad \text{at } \eta = 0, \tag{22}$$

$$f'(\eta) \rightarrow 0, \quad \theta(\eta) \rightarrow 0, \quad \text{as } \eta \rightarrow \infty.$$

5. Skin friction and heat transfer coefficients

For the analysis of surface drag and wall heat transfer, the key physical parameters of interest are the coefficient of skin friction C_f and the reduced Nusselt number Nu_{x^*} . The wall shear stress is expressed as follows:

$$\tau_w = - \left(1 + \frac{1}{\beta} \right) \eta_{nf} \left(\frac{\partial u^*}{\partial y^*} \right)_{y^*=0}. \tag{23}$$

The coefficient of skin friction is expressed as follows:

$$C_f = \frac{\tau_w}{\rho_f U^2}, \tag{24}$$

from the Equations (12), (19), (23) and (24), we obtain

$$C_f \frac{(1 - \phi)^{2.5} Re_{x^*}^{1/2}}{\left(1 + \frac{1}{\beta} \right) (1 + \delta^*)} = -f''(0). \tag{25}$$

The rate of heat transfer at the surface is represented by

$$q_w = -k_{nf} \left(\frac{\partial T^*}{\partial y^*} \right)_{y^*=0}. \tag{26}$$

The Nusselt number is defined as

$$Nu_{x^*} = \frac{x^* q_w}{k_f(T_w - T_\infty)}. \tag{27}$$

Thus, the dimensionless rate of wall heat transfer using Equations (26) and (27) is derived as

$$\frac{Nu_{x^*}}{Re_{x^*}^{1/2}} \left(\frac{k_f}{k_{nf}} \right) = -\theta'(0), \tag{28}$$

where $Re_{x^*} = x^* u_w^*(x^*)/v_f$ in Equations (25) and (28) denotes the local Reynolds number, $Re_{x^*}^{1/2} C_f$ and $Re_{x^*}^{-1/2} Nu_{x^*}$ represent the local skin friction coefficient and the reduced Nusselt number, respectively.

6. Numerical solution using SQLM

The coupled system of Equations (20) and (21), along with the boundary conditions specified in Equation (22), is solved using the SQLM [48–52]. These equations are expressed using nonlinear ordinary differential systems. The SQLM combines quasi-linearization and spectral (Chebyshev) collocation methods, which are reliable techniques. The quasi-linearization method (QLM), proposed by Bellman and Kalaba [53] as an extension of the Newton-Raphson approach, is employed for numerically solving nonlinear boundary-value problems. The core principle of the QLM is to linearize nonlinear variables related to the basic equations. Successive iterations at $r + 1$ and r are assumed to be relatively small and are performed using the Taylor series. The functions F and Θ are denoted as follows:

$$F = (1 + \frac{1}{\beta})(1 + \delta^*)f''' + (1 - \phi)^{2.5}((1 - \phi) + \phi \frac{\rho_s}{\rho_f}) [ff'' - f'^2] - (1 - \phi)^{2.5} \frac{\sigma_{nf}}{\sigma_f} M f', \tag{29}$$

$$\Theta = \frac{k_{nf}}{k_f Pr} \frac{1}{\left((1 - \phi) + \phi \frac{(\rho C_p)_s}{(\rho C_p)_f} \right)} \theta'' + f \theta'. \tag{30}$$

Using Equations (29) and (30), the error function for this iterative procedure is designed as follows:

$$\begin{aligned} R_f &= a_{3,r} f'''_{r+1} + a_{2,r} f''_{r+1} + a_{1,r} f'_{r+1} + a_{0,r} f_{r+1} - F_r, \\ R_\theta &= b_{2,r} \theta''_{r+1} + b_{1,r} \theta'_{r+1} + b_{0,r} \theta_{r+1} + b_{0,r}^* f_{r+1} - \Theta_r, \end{aligned} \tag{31}$$

with relevant boundary conditions

$$\begin{aligned} f_{r+1}(\eta) &= 0, \quad f'_{r+1}(\eta) = 1, \quad \theta_{r+1}(0) = 1, \quad \text{at } \eta = 0, \\ f'_{r+1}(\eta) &\rightarrow 0, \quad \theta_{r+1}(\eta) \rightarrow 0, \quad \text{as } \eta \rightarrow \infty. \end{aligned} \tag{32}$$

The corresponding coefficients of Equation (31) are as follows

$$\begin{aligned} a_{0,r} &= (1 - \phi)^{2.5} \left((1 - \phi) + \phi \frac{\rho_s}{\rho_f} \right) f''_r, \\ a_{1,r} &= -2(1 - \phi)^{2.5} \left((1 - \phi) + \phi \frac{\rho_s}{\rho_f} \right) f'_r + (1 - \phi)^{2.5} \left[1 + \frac{3 \left(\frac{\sigma_s}{\sigma_f} - 1 \right) \phi}{\left(\frac{\sigma_s}{\sigma_f} + 2 \right) - \left(\frac{\sigma_s}{\sigma_f} - 1 \right) \phi} \right] M, \\ a_{2,r} &= (1 - \phi)^{2.5} \left((1 - \phi) + \phi \frac{\rho_s}{\rho_f} \right) f_r, \quad a_{3,r} = (1 + \frac{1}{\beta})(1 + \delta^*), \\ b_{0,r} &= 0, \quad b_{1,r} = f_r, \quad b_{2,r} = \frac{k_{nf}}{k_f Pr} \left((1 - \phi) + \phi \frac{(\rho C_p)_s}{(\rho C_p)_f} \right)^{-1}, \quad \text{and } b_{0,r}^* = \theta'_r. \end{aligned}$$

The initial approximation for this iterative procedure is applied as

$$f_0(\eta) = 1 - e^{-\eta} \text{ and } \theta_0 = e^{-\eta}.$$

The QLM is applied to Equations (20) and (21), and the SQLM, a competent iterative numerical method, is executed using the following procedure for a linearly coupled differential system of equations with a variable coefficient. The transformation of η into $[0, J]$, where $J \in Z^*$ is the boundary region limit, is mapped as $\eta = J(\chi + 1)/2$ in the computational domain $[-1, 1]$. Chebyshev interpolating polynomials are used to approximate the unknown functions f_{r+1} and θ_{r+1} , followed by Gauss-Lobatto collocation points to find the derivatives of the approximated functions as follows:

$$\bar{\chi}_i = \cos\left(\frac{\pi i}{N}\right), \bar{\chi} = [-1, 1], i = 0, 1, 2, 3, \dots, N, \tag{33}$$

where N is the number of collocation points.

The Chebyshev differentiation matrix D is given as

$$\begin{aligned} \frac{d^n f_{r+1}(\bar{\chi}_i)}{d\bar{\chi}} &= \sum_{k=0}^N D_{ik}^n f_{r+1}(\bar{\chi}_i) = D^n \mathbf{F}, \\ \frac{d^n \theta_{r+1}(\bar{\chi}_i)}{d\bar{\chi}} &= \sum_{k=0}^N D_{ik}^n \theta_{r+1}(\bar{\chi}_i) = D^n \theta, \end{aligned} \tag{34}$$

where $\mathbf{D} = \frac{2D}{J}$, $\mathbf{F} = [f_{r+1}(\bar{\chi}_0), f_{r+1}(\bar{\chi}_1), f_{r+1}(\bar{\chi}_2), \dots, f_{r+1}(\bar{\chi}_N)]^T$, and

$\theta = [\theta_{r+1}(\bar{\chi}_0), \theta_{r+1}(\bar{\chi}_1), \theta_{r+1}(\bar{\chi}_2), \dots, \theta_{r+1}(\bar{\chi}_N)]^T$.

Using Equations (20), (21) and (31)-(34), the following simultaneous system is obtained at the collocation points:

$$\begin{aligned} C_{11}\mathbf{F}_{r+1} + C_{12}\theta_{r+1} &= \mathbf{R}_f, \\ C_{21}\mathbf{F}_{r+1} + C_{22}\theta_{r+1} &= \mathbf{R}_\theta, \end{aligned}$$

and the matrix set up of the SQLM technique having derivatives of anonymous functions are as follows

$$\begin{bmatrix} C_{11} & C_{12} \\ C_{21} & C_{22} \end{bmatrix} \begin{bmatrix} \mathbf{F}_{r+1} \\ \theta_{r+1} \end{bmatrix} = \begin{bmatrix} \mathbf{R}_f \\ \mathbf{R}_\theta \end{bmatrix}, \tag{35}$$

where

$$C_{11} = \text{diag}[a_{3,r}]\mathbf{D}^3 + \text{diag}[a_{2,r}]\mathbf{D}^2 + \text{diag}[a_{1,r}]\mathbf{D} + \text{diag}[a_{0,r}]I,$$

$$C_{12} = 0_{N+1 \times N+1},$$

$$C_{21} = \text{diag}[b_{0,r}^*]I, \text{ and}$$

$$C_{22} = \text{diag}[b_{2,r}]\mathbf{D}^2 + \text{diag}[b_{1,r}]\mathbf{D}.$$

Here the diagonal matrix labeled as $\text{diag}[\]$, I is the identity matrix and 0 is the zero matrix with order $(N+1) \times (N+1)$. The solution is obtained by solving the matrix system (35) in accordance with the boundary conditions (32):

When addressing practical challenges in fluid dynamics, it was observed that these issues are correlated with various physical processes. Consequently, these challenges compelled the researchers to tackle intricate, multi-ordered nonlinear differential equations. The process of finding solutions became notably more time-consuming and intricate over time. Occasionally, this approach exhibited slow convergence or even failed to yield a solution. However, it was reported that the utilization of SQLM demonstrates a significantly higher convergence rate compared to existing numerical techniques, and its iterative steps are relatively straightforward to implement [50–52]. The distinctive feature of SQLM, contributing to its widespread acceptance as a numerical technique, was reported to be its ability to break down a complex set of nonlinear equations into smaller subsystems that are inherently more manageable. The residual errors are constructed as follows:

$$\begin{aligned} \text{Res}(f) &= || \Delta_f [F_r, \theta_r] ||_\infty, \\ \text{Res}(\theta) &= || \Delta_\theta [F_r, \theta_r] ||_\infty, \end{aligned} \tag{36}$$

where Δ_f and Δ_θ represents the nonlinear Equations (21) and (22), and F_r and θ_r , represents the SQLM solutions at the nodes. Also the residue errors in Equation (36) are clearly shown in Fig. 2. It is noticed that after the 5th or 6th iteration the related error is consistent and the rapid convergence rate falls after the 5th or 6th iteration.

7. SQLM validation

The governing system of equations describing the mass, momentum, and energy of a non-Newtonian (Casson)-based homogeneous Fe_3O_4 nanofluid is solved using a spectral QLM. To validate the accuracy of this study, it is compared with the results of Wang [54] and Gorla et al. [55] (see Table 2). The results presented in Table 2 demonstrate a good agreement with the benchmark results. In this study, a tolerance error of $\epsilon = 10^{-10}$ was employed, and the residues were used to test accuracy had an error value of 10^{-10} for momentum and 10^{-12} for the energy equations (see Fig. 2).

8. Results and discussion

The computational results of the dimensionless governing ordinary differential equations obtained using the SQLM are discussed in detail. Graphical plots are used to investigate the impacts of the isotropic MFD viscosity (δ), nanoparticle volume fraction (ϕ), magnetic parameter (M), and Casson parameter (β) on the natural convection of the boundary layer flow of a sodium alginate-based Fe_3O_4 -nanofluid over an impermeable stretching surface. The following values were held constant throughout the investigation while studying the impacts of individual parameters: $Pr = 6.45$, $M = 1$, $\phi = 0.1$, $\beta = 0.1$ and $\delta^* = 0.15$. Additionally, $N = 100$ collocation points were used to emphasize individuality.

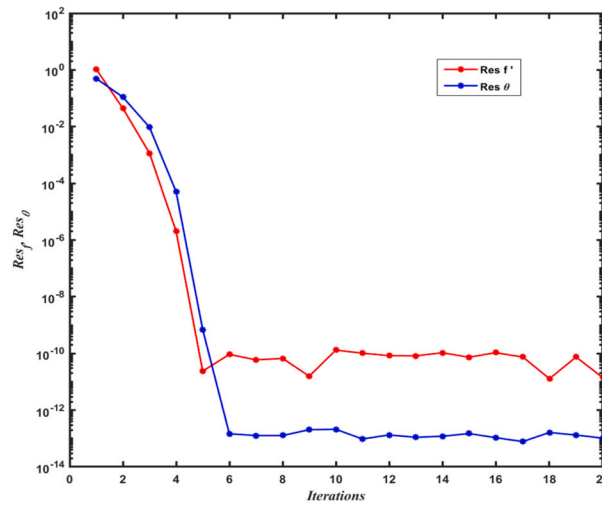


Fig. 2. The residues of velocity and temperature profiles.

Table 2
Comparison of variations of $-\theta'(0)$.

Pr	Wang [54]	Gorla et al. [55]	Present Study
0.07	0.0656	0.0656	0.065806
0.2	0.1691	0.1691	0.169088
0.7	0.4539	0.4539	0.453916
2	0.9114	0.9114	0.911354
7	1.8971	1.8904	1.897186

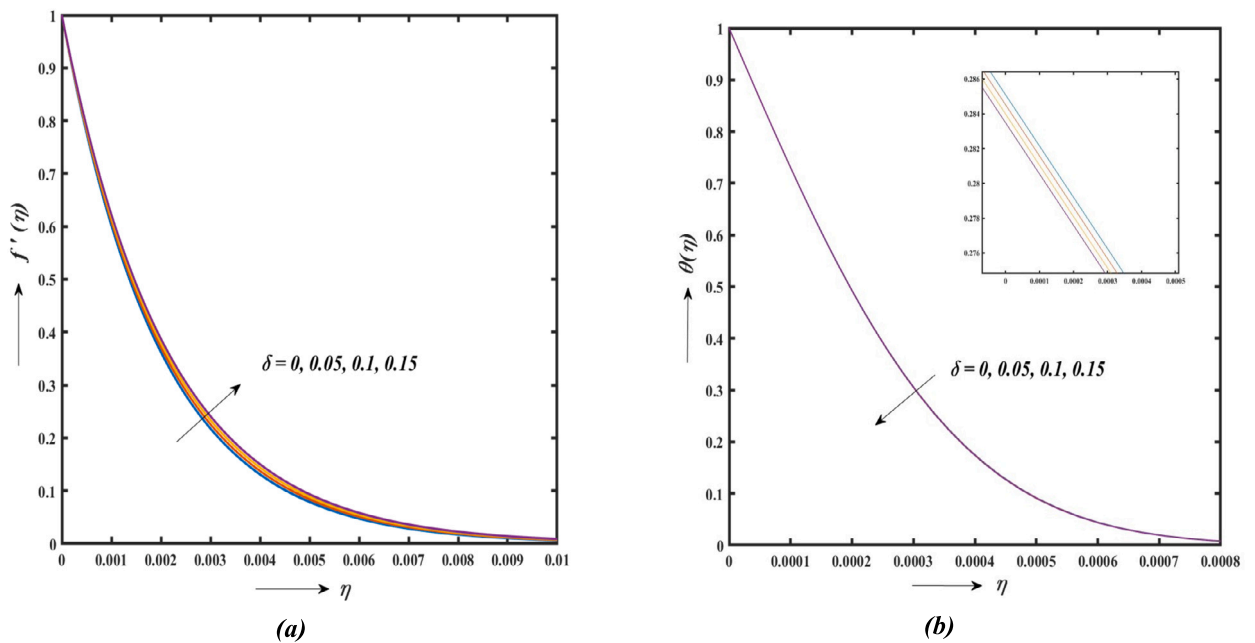


Fig. 3. Effect of MFD viscosity parameter on (a) velocity profile & (b) temperature profile.

Figs. 3(a) and 3(b) illustrate the effects of the isotropic MFD viscosity parameter on the velocity and thermal profiles of the Casson-based Fe_3O_4 nanofluid, respectively. The MFD viscosity parameter primarily influences the velocity and momentum boundary layers than the temperature and thermal boundary layer due to the negligible effects of viscous and ohmic dissipations in the model. Fig. 3(a) presents the results for two cases: fluid flow with viscosity dependent on the magnetic field, and fluid flow with viscosity independent of the magnetic field. Increasing the MFD viscosity accelerated the nanofluid velocity, resulting in an expanded momentum boundary

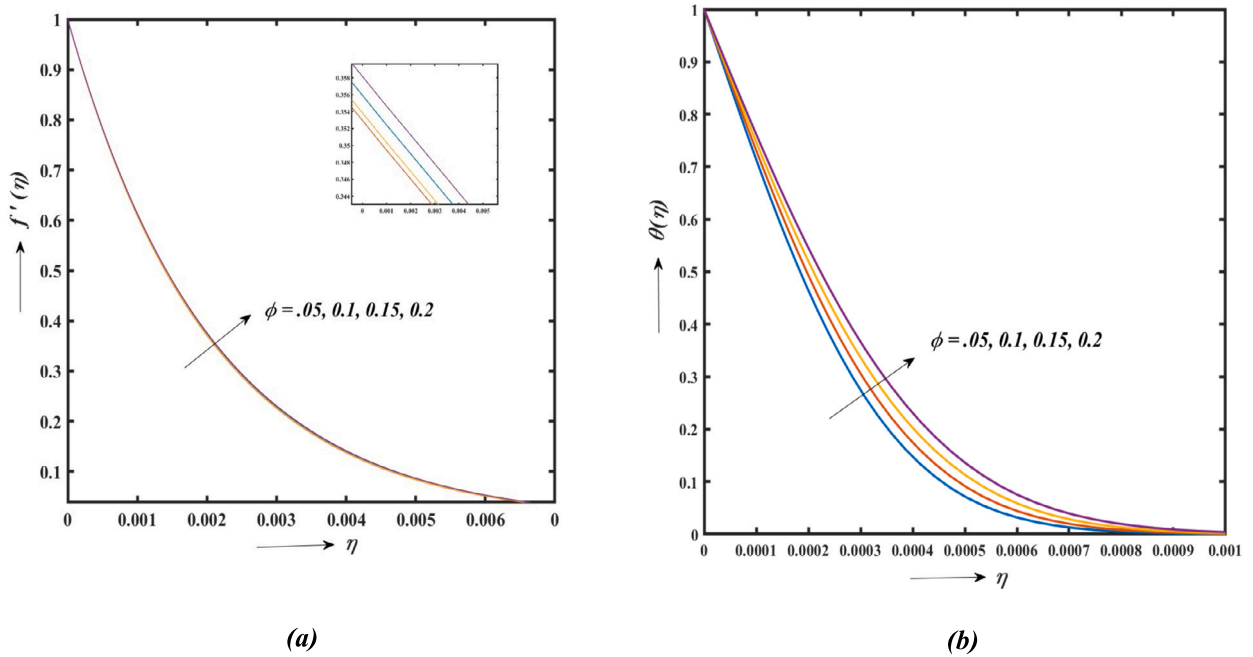


Fig. 4. Effect of volume fraction of Fe_3O_4 nanoparticles on (a) velocity profile & (b) temperature profile.

layer. This is attributed to the increased MFD viscosity when exposed to a transverse magnetic field. This led to a reduction in the shear stress of the Fe_3O_4 nanofluid and a stretching of the surface interface parallel to the magnetic field, potentially increasing velocity and momentum boundary layers. Fig. 3(b) shows that an increase in the MFD viscosity parameter leads to a slight decrease in both the temperature profile and thickness of the thermal boundary layer.

The influence of the volume fraction of Fe_3O_4 nanoparticles on velocity and temperature profiles of Casson-based nanofluid is depicted in the existence of magnetic field dependent viscosity (see Figs. 4(a) and 4(b)). The volume fraction of nanoparticles affected the thermal profile and thermal boundary layers more than the fluid flow and momentum boundary layer. A marginal increase in the velocity profile was noted, whereas an enhancement was detected due to changes in the nanoparticle volume fraction. This was attributed to the increase in suspension volume fraction, which resulted in a marginal reduction in the wall shear stress and a simultaneous increase in thermal conductivity within the boundary layer region.

Figs. 5(a) and 5(b) demonstrate the impact of the magnetic parameters on the velocity and temperature profiles of the Casson-based Fe_3O_4 nanofluid. Increased magnetic parameters resulted in an improved temperature profile and reduced velocity. This was because the Lorentz force, acting perpendicular to the magnetic field and opposite to the fluid viscosity, affects the nanofluid as the magnetic parameter increased, while the magnetic field strength remained constant.

Figs. 6 and 7 illustrate the impact of the magnetic, MFD viscosity, and Casson parameters on significant physical quantities: the local skin friction coefficient and reduced Nusselt number. The numerical outcomes of the local skin friction coefficient and reduced Nusselt number are displayed in Table. 3. The findings indicated an inverse relationship between the local skin friction coefficient and the MFD viscosity, whereas a direct relationship existed with the magnetic field and Casson parameters (see Figs. 6(a) and 6(b)). The increased viscosity parameter, dependent on the magnetic field, led to an increase in the reduced Nusselt number (see Figs. 7(a) and 7(b)). Furthermore, the Nusselt number decreased as the magnetic and Casson parameters increased. It was observed that an increase in the MFD viscosity parameter has the potential to enhance the heat transfer rate at the stretching boundary, while reducing skin friction can increase the flow velocity at the stretching sheet. The MFD viscosity was found to contribute to skin friction reduction and enhancement of the rate of heat transfer within the boundary layer of the Casson-based nanofluid containing Fe_3O_4 , generated by a stretching sheet.

9. Conclusion

This study investigated the impact of MFD viscosity on the boundary layer flow of a nanofluid across a stretched surface. The SQLM and Lie group approaches were adopted to explore the impact of the MFD on the boundary layer flow of a non-Newtonian-based Fe_3O_4 nanofluid over an impermeable stretching surface. The key findings of the current numerical investigations were:

- The presence of MFD viscosity led to significant variations in the velocity profile of the Casson-based Fe_3O_4 nanofluid. Increasing the MFD viscosity parameter accelerated the nanofluid velocity, resulting in an expansion of the momentum boundary layer thickness.

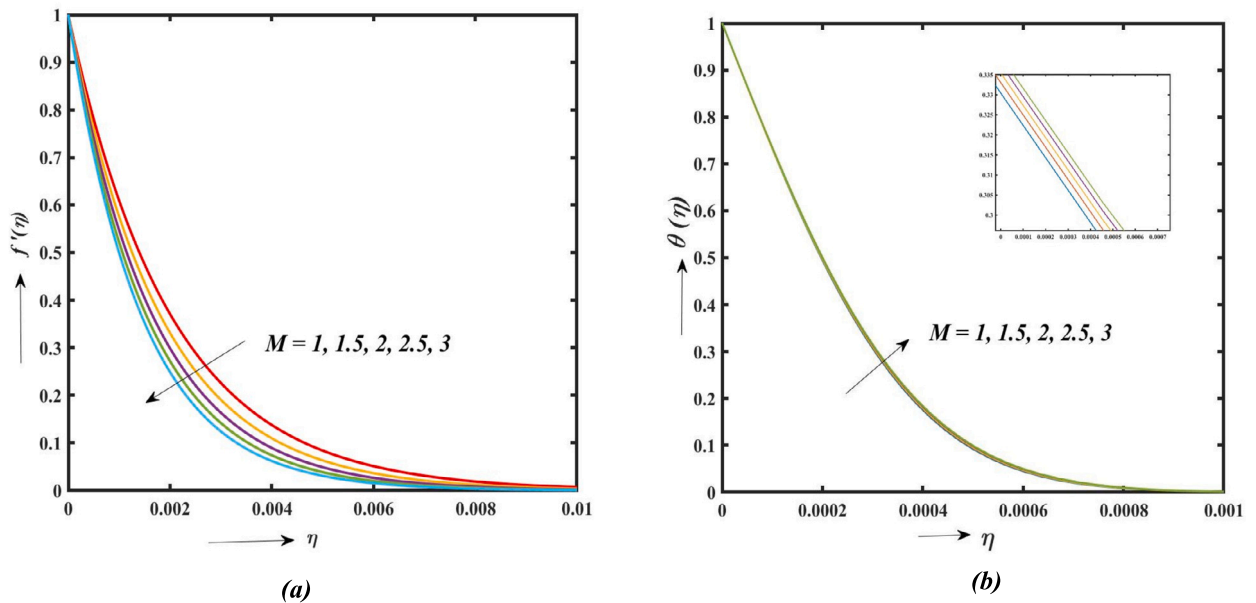


Fig. 5. Effect of magnetic parameter on (a) velocity profile & (b) temperature profile.

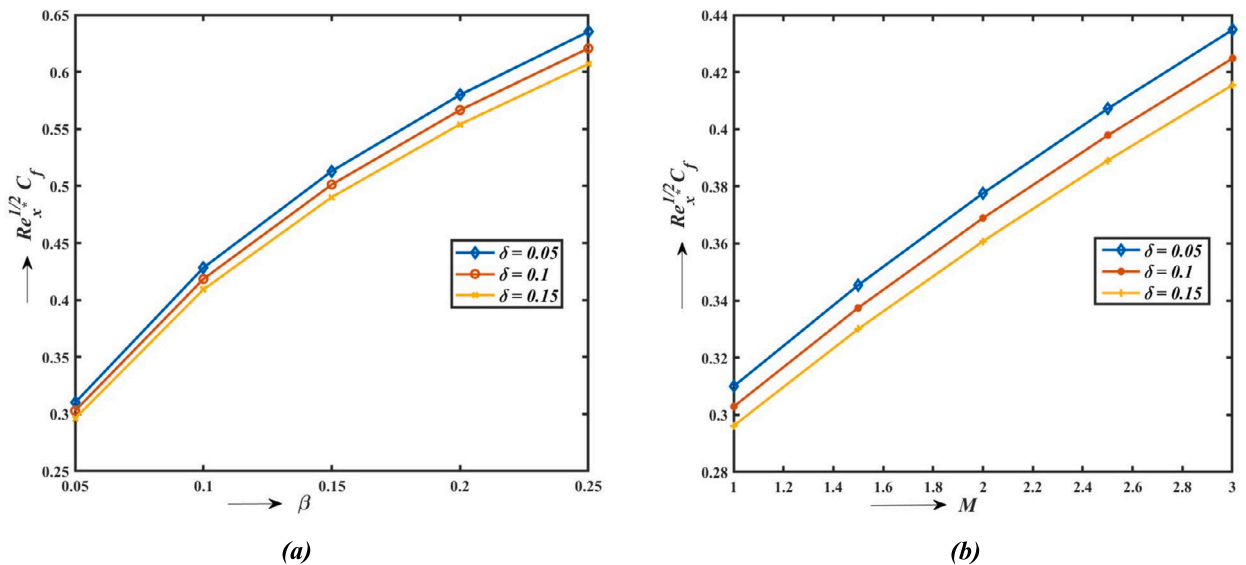


Fig. 6. The local skin friction coefficient variations (a) Effect of viscosity parameter & Casson parameter (b) Effect of viscosity parameter & magnetic parameter.

- The thermal boundary layer thickness was suppressed as the magnetic field parameter increased, owing to the effects of MFD viscosity.
- Increasing the MFD viscosity parameter resulted in an increase in the dimensionless quantities, specifically the local skin friction and the reduced Nusselt number.
- The numerical results for skin friction and reduced Nusselt number presented in this study can serve as benchmark results for future comparative studies investigating the effects of MFD viscosity on boundary layer flows.

CRedit authorship contribution statement

N. Vishnu Ganesh: Writing – original draft, Visualization, Validation, Methodology, Investigation, Formal analysis, Conceptualization. **B. Rajesh:** Writing – review & editing, Writing – original draft, Validation, Methodology, Formal analysis, Conceptualization. **Qasem M. Al-Mdallal:** Writing – review & editing, Software, Methodology, Funding acquisition, Conceptualization. **Hillary Muzara:** Writing – review & editing, Supervision, Methodology, Formal analysis, Conceptualization.

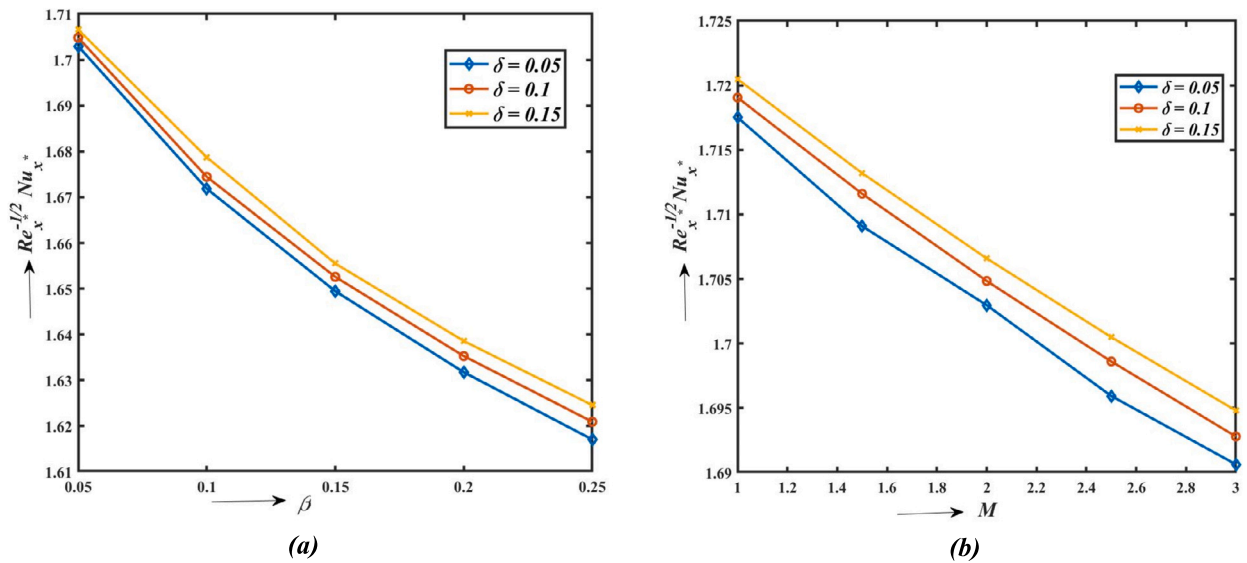


Fig. 7. The reduced Nusselt number variations (a) Effect of MFD viscosity parameter & Casson parameter & (b) Effect of MFD viscosity parameter & magnetic parameter.

Table 3
Values of local Skin friction and reduced Nusselt number.

M	β	δ^*	$-f''(0)$	$-\theta'(0)$
1	0.05	0.05	0.3099734	1.7175150
		0.10	0.3028466	1.7190461
		0.15	0.2961898	1.7204759
	0.10	0.05	0.4282898	1.6920365
		0.10	0.4184428	1.6941611
		0.15	0.4092451	1.6961450
	0.15	0.05	0.5130159	1.6737259
		0.10	0.5012208	1.6762781
		0.15	0.4902037	1.6786611
2	0.05	0.05	0.3775573	1.7029748
		0.10	0.3688767	1.7048444
		0.15	0.3607685	1.7065901
	0.10	0.05	0.5216705	1.6718526
		0.10	0.5096764	1.6744486
		0.15	0.4984734	1.6787254
	0.15	0.05	0.6248695	1.6494757
		0.10	0.6105027	1.6525951
		0.15	0.5970834	1.6555076

Declaration of competing interest

The authors declare that they have no known competing financial interests or personal relationships that could have appeared to influence the work reported in this paper.

Acknowledgements

The authors wish to express his sincere thanks to the honorable referees and the editor for their valuable comments and suggestions to improve the quality of the paper. Additionally, all authors would like to express their gratitude to the United Arab Emirates University, Al Ain, UAE, for providing financial support with Grant No. 12S122.

References

[1] F.K. Tsou, E.M. Sparrow, R.J. Goldstein, Flow and heat transfer in the boundary layer on a continuous moving surface, *Int. J. Heat Mass Transf.* 10 (2) (1967) 219–235.

- [2] L.J. Crane, Flow past a stretching plate, *Z. Angew. Math. Phys.* 21 (1970) 645–647.
- [3] F.N. Lin, S.Y. Chern, Laminar boundary-layer flow of non-Newtonian fluid, *Int. J. Heat Mass Transf.* 22 (10) (1979) 1323–1329.
- [4] B.K. Dutta, P. Roy, A.S. Gupta, Temperature field in flow over a stretching sheet with uniform heat flux, *Int. Commun. Heat Mass Transf.* 12 (1) (1985) 89–94.
- [5] H. Xu, S.J. Liao, Laminar flow and heat transfer in the boundary-layer of non-Newtonian fluids over a stretching flat sheet, *Comput. Math. Appl.* 57 (9) (2009) 1425–1431.
- [6] T. Javed, N. Ali, Z. Abbas, M. Sajid, Flow of an Eyring-Powell non-Newtonian fluid over a stretching sheet, *Chem. Eng. Commun.* 200 (3) (2013) 327–336.
- [7] A.A. Hakeem, N.V. Ganesh, B. Ganga, Effect of heat radiation in a Walter's liquid B fluid over a stretching sheet with non-uniform heat source/sink and elastic deformation, *J. King Saud Univ., Eng. Sci.* 26 (2) (2014) 168–175.
- [8] S. Nasir, Z. Shah, S. Islam, E. Bonyah, T. Gul, Darcy Forchheimer nanofluid thin film flow of SWCNTs and heat transfer analysis over an unsteady stretching sheet, *AIP Adv.* 9 (1) (2019).
- [9] T. Gul, S. Nasir, A.S. Berrouk, Z. Raizah, W. Alghamdi, I. Ali, A. Bariq, Simulation of the water-based hybrid nanofluids flow through a porous cavity for the applications of the heat transfer, *Sci. Rep.* 13 (1) (2023) 7009.
- [10] A.S. Alnahdi, S. Nasir, T. Gul, Ternary Casson hybrid nanofluids in convergent/divergent channel for the application of medication, *Therm. Sci.* 27 (Spec. issue 1) (2023) 67–76.
- [11] M.V. Reddy, P. Lakshminarayana, K. Vajravelu, A comparative study of MHD non-Newtonian fluid flows with the effects of chemical reaction and radiation over a stretching sheet, *Comput. Therm. Sci. Int. J.* 13 (5) (2021).
- [12] K. Sarada, R.J.P. Gowda, I.E. Sarris, R.N. Kumar, B.C. Prasannakumara, Effect of magnetohydrodynamics on heat transfer behaviour of a non-Newtonian fluid flow over a stretching sheet under local thermal non-equilibrium condition, *Fluids* 6 (8) (2021) 264.
- [13] N. Abbas, S. Nadeem, M.N. Khan, Numerical analysis of unsteady magnetized micropolar fluid flow over a curved surface, *J. Therm. Anal. Calorim.* 147 (11) (2022) 6449–6459.
- [14] S.U. Choi, J.A. Eastman, Enhancing thermal conductivity of fluids with nanoparticles (No. ANL/MSD/CP-84938; CONF-951135-29), Argonne National Lab. (ANL), Argonne, IL (United States), 1995.
- [15] M. Hamid, M. Usman, Z.H. Khan, R. Ahmad, W. Wang, Dual solutions and stability analysis of flow and heat transfer of Casson fluid over a stretching sheet, *Phys. Lett. A* 383 (20) (2019) 2400–2408.
- [16] M. Mustafa, T. Hayat, P. Ioan, A. Hendi, Stagnation-point flow and heat transfer of a Casson fluid towards a stretching sheet, *Z. Naturforsch. A* 67 (1–2) (2012) 70–76.
- [17] N.V. Ganesh, Q.M. Al-Mdallal, R. Kalaivanan, K. Reena, Arrhenius kinetics driven nonlinear mixed convection flow of Casson liquid over a stretching surface in a Darcian porous medium, *Heliyon* 9 (6) (2023).
- [18] V. Bianco, O. Manca, S. Nardini, K. Vafai (Eds.), *Heat Transfer Enhancement with Nanofluids*, CRC Press, 2015.
- [19] N.V. Ganesh, Q.M. Al-Mdallal, H.F. Öztop, R. Kalaivanan, Analysis of natural convection for a Casson-based multiwall carbon nanotube nanofluid in a partially heated wavy enclosure with a circular obstacle in the presence of thermal radiation, *J. Adv. Res.* 39 (2022) 167–185.
- [20] W. Jamsheed, M. Goodarzi, M. Prakash, K.S. Nisar, M. Zakarya, A.H. Abdel-Aty, Evaluating the unsteady Casson nanofluid over a stretching sheet with solar thermal radiation: an optimal case study, *Case Stud. Therm. Eng.* 26 (2021) 101160.
- [21] J.V. Tawade, C.N. Guled, S. Noeiaghdam, U. Fernandez-Gamiz, V. Govindan, S. Balamuralitharan, Effects of thermophoresis and Brownian motion for thermal and chemically reacting Casson nanofluid flow over a linearly stretching sheet, *Results Eng.* 15 (2022) 100448.
- [22] P.M. Bhavana, G.P. Vanitha, U.S. Mahabaleshwar, B. Souayah, Effect of magnetohydrodynamic Casson fluid flow on the stretching/shrinking surface, *Z. Angew. Math. Mech. (Zeitschrift für Angewandte Mathematik und Mechanik)* (2023) e202200523.
- [23] A.A. Hakeem, P. Renuka, N.V. Ganesh, R. Kalaivanan, B. Ganga, Influence of inclined Lorentz forces on boundary layer flow of Casson fluid over an impermeable stretching sheet with heat transfer, *J. Magn. Magn. Mater.* 401 (2016) 354–361.
- [24] S. Nasir, S. Islam, T. Gul, Z. Shah, M.A. Khan, W. Khan, A.Z. Khan, S. Khan, Three-dimensional rotating flow of MHD single wall carbon nanotubes over a stretching sheet in presence of thermal radiation, *Appl. Nanosci.* 8 (2018) 1361–1378.
- [25] H.B. Lanjwani, S. Saleem, M.S. Chandio, M.I. Anwar, N. Abbas, Stability analysis of triple solutions of Casson nanofluid past on a vertical exponentially stretching/shrinking sheet, *Adv. Mech. Eng.* 13 (11) (2021) 16878140211059679.
- [26] N. Abbas, W. Shatanawi, Heat and mass transfer of micropolar-Casson nanofluid over vertical variable stretching rigid sheet, *Energies* 15 (14) (2022) 4945.
- [27] A.A. Hakeem, N.V. Ganesh, B. Ganga, Magnetic field effect on second order slip flow of nanofluid over a stretching/shrinking sheet with thermal radiation effect, *J. Magn. Magn. Mater.* 381 (2015) 243–257.
- [28] U. Khan, A. Zaib, A. Ishak, I. Waini, I. Pop, S. Elattar, A.M. Abed, Stagnation point flow of a water-based graphene-oxide over a stretching/shrinking sheet under an induced magnetic field with homogeneous-heterogeneous chemical reaction, *J. Magn. Magn. Mater.* 565 (2023) 170287.
- [29] P.P. Gogoi, S.K. Singh, S. Maity, Two layer thin film flow over a stretching sheet with uniform transverse magnetic field, *J. Magn. Magn. Mater.* 565 (2023) 170204.
- [30] C. Sulochana, G.P. Ashwinkumar, N. Sandeep, Similarity solution of 3D Casson nanofluid flow over a stretching sheet with convective boundary conditions, *J. Niger. Math. Soc.* 35 (1) (2016) 128–141.
- [31] Z. Sabir, R. Akhtar, Z. Zhiyu, M. Umar, A. Imran, H.A. Wahab, et al., A computational analysis of two-phase Casson nanofluid passing a stretching sheet using chemical reactions and gyrotactic microorganisms, *Math. Probl. Eng.* 2019 (2019).
- [32] S. Nadeem, R.U. Haq, N.S. Akbar, MHD three-dimensional boundary layer flow of Casson nanofluid past a linearly stretching sheet with convective boundary condition, *IEEE Trans. Nanotechnol.* 13 (1) (2013) 109–115.
- [33] M. Mustafa, J.A. Khan, Model for flow of Casson nanofluid past a non-linearly stretching sheet considering magnetic field effects, *AIP Adv.* 5 (7) (2015).
- [34] A. Khan, D. Khan, I. Khan, F. Ali, F.U. Karim, M. Imran, MHD flow of sodium alginate-based Casson type nanofluid passing through a porous medium with Newtonian heating, *Sci. Rep.* 8 (1) (2018) 8645.
- [35] S.S. Ghadikolaei, K. Hosseinzadeh, D.D. Ganji, B. Jafari, Nonlinear thermal radiation effect on magneto Casson nanofluid flow with Joule heating effect over an inclined porous stretching sheet, *Case Stud. Therm. Eng.* 12 (2018) 176–187.
- [36] A.C. Venkata Ramudu, K. Anantha Kumar, V. Sugunamma, N. Sandeep, Heat and mass transfer in MHD Casson nanofluid flow past a stretching sheet with thermophoresis and Brownian motion, *Heat Transf.* 49 (8) (2020) 5020–5037.
- [37] F.A. Alwawi, H.T. Alkasasbeh, A.M. Rashad, R. Idris, MHD natural convection of sodium alginate Casson nanofluid over a solid sphere, *Results Phys.* 16 (2020) 102818.
- [38] L. Panigrahi, J. Panda, K. Swain, G.C. Dash, Heat and mass transfer of MHD Casson nanofluid flow through a porous medium past a stretching sheet with Newtonian heating and chemical reaction, *Karbala Int. J. Mod. Sci.* 6 (3) (2020) 11.
- [39] W. Jamsheed, E.K. Akgül, K.S. Nisar, Keller box study for inclined magnetically driven Casson nanofluid over a stretching sheet: single phase model, *Phys. Scr.* 96 (6) (2021) 065201.
- [40] Y. Suresh Kumar, S. Hussain, K. Raghunath, F. Ali, K. Guedri, S.M. Eldin, M.I. Khan, Numerical analysis of magnetohydrodynamics Casson nanofluid flow with activation energy, Hall current and thermal radiation, *Sci. Rep.* 13 (1) (2023) 4021.
- [41] B.N. Reddy, P. Maddileti, Casson nanofluid and Joule parameter effects on variable radiative flow of MHD stretching sheet, *Partial Differ. Equ. Appl. Math.* 7 (2023) 100487.
- [42] P.R. Sekhar, S. Sreedhar, S.M. Ibrahim, P.V. Kumar, Radiative heat source fluid flow of MHD Casson nanofluid over a non-linear inclined surface with Soret and Dufour effects, *CFD Lett.* 15 (7) (2023) 42–60.

- [43] S. Rani, H.A.M. Al-Sharifi, M.S. Zannon, A. Hussanan, Z. Ullah, Nanoparticle shape effect on a sodium–alginate based Cu–nanofluid under a transverse magnetic field, *Fluid Dyn. Mater. Proc.* 19 (7) (2023).
- [44] M. Sheikholeslami, M.M. Rashidi, T. Hayat, D.D. Ganji, Free convection of magnetic nanofluid considering MFD viscosity effect, *J. Mol. Liq.* 218 (2016) 393–399.
- [45] M. Sheikholeslami, M.K. Sadoughi, Numerical modeling for Fe₃O₄-water nanofluid flow in porous medium considering MFD viscosity, *J. Mol. Liq.* 242 (2017) 255–264.
- [46] M. Molana, A.S. Dogonchi, T. Armaghani, A.J. Chamkha, D.D. Ganji, I. Tili, Investigation of hydrothermal behavior of Fe₃O₄-H₂O nanofluid natural convection in a novel shape of porous cavity subjected to magnetic field dependent (MFD) viscosity, *J. Energy Storage* 30 (2020) 101395.
- [47] P.G. Metri, E. Guariglia, S. Silvestrov, January. Lie group analysis for MHD boundary layer flow and heat transfer over stretching sheet in presence of viscous dissipation and uniform heat source/sink, in: *AIP Conference Proceedings* (vol. 1798, no. 1), AIP Publishing, 2017.
- [48] O.A. Bég, S.S. Motsa, A. Kadir, T.A. Bég, M.N. Islam, Spectral quasilinear numerical simulation of micropolar convective wall plumes in high permeability porous media, *J. Eng. Thermophys.* 25 (2016) 576–599.
- [49] D. Srinivasacharya, S.S. Motsa, O. Surender, Numerical study of free convection in a doubly stratified non-Darcy porous medium using spectral quasilinearization method, *Int. J. Nonlinear Sci. Numer. Simul.* 16 (3–4) (2015) 173–183.
- [50] S. Shateyi, H. Muzara, On the numerical analysis of unsteady MHD boundary layer flow of Williamson fluid over a stretching sheet and heat and mass transfers, *Computation* 8 (2) (2020) 55.
- [51] S. Shateyi, H. Muzara, A numerical analysis on the unsteady flow of a thermomagnetic reactive Maxwell nanofluid over a stretching/shrinking sheet with ohmic dissipation and Brownian motion, *Fluids* 7 (8) (2022) 252.
- [52] S. Shateyi, H. Muzara, Unsteady MHD Blasius and Sakiadis flows with variable thermal conductivity in the presence of thermal radiation and viscous dissipation, *Front. Heat Mass Transf.* 14 (2020).
- [53] R.E. Bellman, R.E. Kalaba, *Quasilinearization and nonlinear boundary-value problems*, 1965.
- [54] C.Y. Wang, Free convection on a vertical stretching surface, *Z. Angew. Math. Mech. (Zeitschrift für Angewandte Mathematik und Mechanik)* 69 (11) (1989) 418–420.
- [55] R.S. Reddy Gorla, I. Sidawi, Free convection on a vertical stretching surface with suction and blowing, *Appl. Sci. Res.* 52 (1994) 247–257.